

AnimateAnywhere: Rouse the Background in Human Image Animation

<https://animateanywhere.github.io/>

Xiaoyu Liu
Harbin Institute of Technology
liuxiaoyu1104@gmail.com

Mingshuai Yao
Harbin Institute of Technology
ymsoyosmy@gmail.com

Yabo Zhang
Harbin Institute of Technology
hitzhangyabo2017@gmail.com

Xianhui Lin
xhlin129@gmail.com

Peiran Ren
renpeiran@gmail.com

Xiaoming Li
Nanyang Technological University
csxmli@gmail.com

Ming Liu
Harbin Institute of Technology
csmlu@outlook.com

Wangmeng Zuo
Harbin Institute of Technology
wmzuo@hit.edu.cn

Abstract

Human image animation aims to generate human videos of given characters and backgrounds that adhere to the desired pose sequence. However, existing methods focus more on human actions while neglecting the generation of background, which typically leads to static results or inharmonious movements. The community has explored camera pose-guided animation tasks, yet preparing the camera trajectory is impractical for most entertainment applications and ordinary users. As a remedy, we present an AnimateAnywhere framework, rousing the background in human image animation without requirements on camera trajectories. In particular, based on our key insight that the movement of the human body often reflects the motion of the background, we introduce a background motion learner (BML) to learn background motions from human pose sequences. To encourage the model to learn more accurate cross-frame correspondences, we further deploy an epipolar constraint on the 3D attention map. Specifically, the mask used to suppress geometrically unreasonable attention is carefully constructed by combining an epipolar mask and the current 3D attention map. Extensive experiments demonstrate that our AnimateAnywhere effectively learns the background motion from human pose sequences, achieving state-of-the-art performance in generating human animation results with vivid and realistic backgrounds. The source code and model will be available at <https://github.com/liuxiaoyu1104/AnimateAnywhere>.

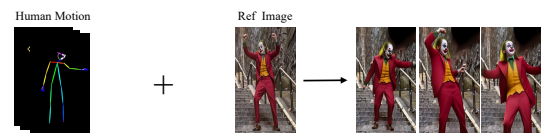
Keywords

Video Generation, Human Animation, Background Motion

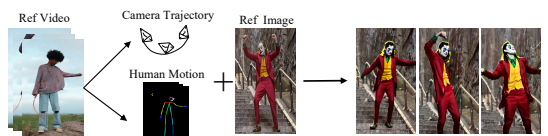
1 Introduction

Human image animation has become a popular task focused on transforming source character images into realistic videos based on human pose sequences. This technique has a wide range of potential applications, including in entertainment videos, artistic creation, and virtual characters.

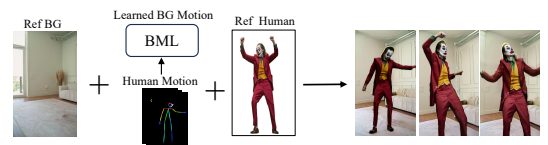
Recent advancements in generative diffusion models have significantly advanced the field of image animation [12, 24, 25, 32, 40, 42], enabling the creation of highly realistic and controllable human



(a) Human animation with static backgrounds



(b) Human animation with dynamic backgrounds guided by background motion conditions



(c) Human animation with dynamic backgrounds synchronized with human poses

Figure 1: Comparison with existing paradigms of human image animation. (a) Human animation with static backgrounds: Animate Anyone [12], MagicAnimate [32], Champ [42], and *etc.* They only generate static backgrounds. (b) Human animation with dynamic backgrounds guided by background motion conditions: Humanvid [28], Liu *et al.* [15], and *etc.* They extract background motion conditions of reference videos to guide the movement of the background. However, extracting background motion conditions paired with human poses heavily relies on reference videos, which are often unavailable in practice. (c) Ours: Human animation with dynamic backgrounds synchronized with human poses. Our paradigm learns the background movements that are harmonious with the human poses for human animation.

image animation, particularly in terms of identity preservation and motion consistency. Despite these advancements, most existing human image animation methods focus on improving the generation quality of foreground humans while leaving the background static or unconstrained. However, in practice, the photographers usually need to adjust the cameras to better capture human movements,

postures, and *etc.*, which results in background changes. Thus, the static or disharmonious backgrounds are insufficient to meet the requirements for realistic and diverse human video generation.

To address this issue, one possible solution is to employ control signals to guide background motion. For example, Humanvid [28] controls the background motion via camera trajectories estimated from the reference videos, while Liu *et al.* [15] leverage sparse tracking points and human pose sequences to independently control background and foreground motions. However, these methods typically acquire background control signals from a reference video, which is unavailable in many scenarios. Although camera trajectories can be manually designed, this easily results in disharmony between human and background motion. It requires professional skills and is redundant for most applications and ordinary users. Additionally, another limitation of these methods is that a reference image with both the human and the background is required.

To overcome the above limitations of existing human image animation methods, this work proposes AnimateAnywhere, a novel framework that generates videos with harmonious human and background motion controlled solely by human pose sequences, without additional camera control conditions. As shown in fig. 1, the key idea of our AnimateAnywhere is to identify the background motion from human pose sequences. We argue that human pose sequences can imply background motion. For instance, when a person appears larger or smaller across frames while remaining stationary, the background typically exhibits a corresponding zoom-in or zoom-out motion. Moreover, if a person walks to the left while remaining centered in the frame, it means that the camera is moving left, and the background should shift accordingly. By observing the relative changes in a person’s size and position across frames, as well as the type of human actions that can also be inferred from the human pose sequence, we can estimate both the direction and extent of background motion.

Specifically, we build the AnimateAnywhere framework upon a pre-trained image-to-video model (*i.e.*, CogVideoX [34]) and independently inject a reference human image, a reference background image, and a human pose sequence into the generation process. Thus, AnimateAnywhere supports free combinations of reference humans, backgrounds, and pose sequences, enabling highly flexible and controllable video generation. To realize the key idea of AnimateAnywhere, we propose the Background Motion Learner (BML) module, which learns background motion from the latent features of human pose sequences by applying LoRA [11] on the 3D-attention-based block. Moreover, although 3D full attention allows each background pixel to attend to any other pixel from all frames, this highly free attention manner also brings difficulties to optimization, easily resulting in geometrically inconsistent background generation. To further improve the cross-frame geometric consistency of the background, we propose an adaptive epipolar constraint for the 3D attention map. Therein, a mask used for suppressing geometrically unreasonable attention is elaborately designed from an epipolar mask and the current 3D attention map.

As shown in fig. 1, our AnimateAnywhere can generate realistic videos with harmonious human and background motion, without additional background motion control conditions. Extensive experiments conducted on the constructed datasets show that our

AnimateAnywhere outperforms state-of-the-art methods, demonstrating the effectiveness, flexibility, and controllability of generating dynamically harmonious human and background motions. Our contributions are listed as follows.

- We propose AnimateAnywhere, a novel human image animation framework that generates dynamic backgrounds in harmony with human motions, requiring no camera pose information. It also supports flexible combinations of reference humans, backgrounds, and pose sequences.
- We propose a Background Motion Learner (BML) module to predict background motion from human pose sequences and an adaptive epipolar constraint for the 3D attention map to enhance background geometric consistency.
- Our method achieves state-of-the-art performance in the challenging test dataset, demonstrating the effectiveness, flexibility, and controllability for human animation.

2 Related Work

2.1 Human Image Animation

Human image Animation aims to generate coherent human videos from a reference image and a target pose sequence. By leveraging the generative visual capabilities of diffusion models, recent advancements [12, 24, 25, 28, 32, 35, 40, 42] have enabled the generation of high-quality and consistent human animation videos. AnimateAnyone [12] and MagicAnimate [32] introduce a video diffusion model and a reference network for temporal consistency and identity preservation, respectively. Champ [42] incorporates four distinct control signals to provide comprehensive 3D shape and detailed pose guidance. Following these, some works focus on realistic hands [24, 40], efficient temporal modeling [25], or a pose alignment algorithm [22] to further improve the performance of human animation. Animate-X [20] extends animation to diverse character types with a unified framework.

Despite achieving reasonable results in maintaining temporal consistency in humans, these approaches face challenges in generating realistic and dynamic backgrounds. MIMO [17] and AnimateAnyone2 [13] address this challenge by taking the background video directly from a reference video as input. Liu *et al.* [15] extract sparse point tracking from the reference video and use it to guide background animation. Humanvid [28] utilizes a SLAM-based method [21, 26] to estimate an accurate camera trajectory from the original videos and leverages CameraCtrl [6] and Animate Anyone [12] to construct a human animation framework. DynaScene [35] further introduces a multi-task learning approach to enhance the realism of the generated background. In comparison to the existing methods, our AnimateAnywhere predicts the background motion from human pose sequences without the reference video and camera pose extraction during inference.

2.2 Camera Control Video Generation

With the impressive capabilities of video diffusion models [1, 2, 4, 5, 8] in generating high-quality videos, several approaches have focused on achieving controllable video generation by incorporating conditional controls [3, 4, 6, 30, 38]. In this section, we provide a

brief overview of the progress in camera-controllable video generation. AnimateDiff [4] uses MotionLoRA [10] fine-tuning to adapt a pre-trained video model to specific camera movements. Direct-a-video [33] introduces a camera embedder that incorporates three camera parameters, though the limited parameters restrict camera movement to translations and zooms. Following this, MotionCtrl [29] incorporates rotation and translation matrices derived from extrinsic camera parameters, enabling the generation of videos with more complex camera motions. CameraCtrl [6] leverages Plücker coordinates to represent camera poses, allowing for geometric interpretations at the pixel level. Recent advances further enhance the geometric consistency of generated videos by epipolar constraints or 3D reconstruction. CamCo [31] applies epipolar constraints to ensure consistency between generated frames and a single reference frame only. CAMI2V [39] extends epipolar constraints onto all frames to account for scenarios where frames lack overlapping regions with the reference frame. CamTrol [9] models camera movements through explicit 3D point clouds. Building on the epipolar constraint used in CAMI2V [39], we introduce an adaptive epipolar constraint on the 3D attention map of the background regions.

3 Method

Given a human image I_{hum} , a background image I_{bg} , and a human pose sequence $\mathbf{P}^{1:N}$, AnimateAnywhere generates a video with synchronized human and background motion, guided solely by the pose sequence without explicit background motion control. Firstly, the preliminaries of AnimateAnywhere, including our base model CogVideoX [34] and 3D Full Attention, are introduced in section 3.1. Additionally, we introduce the Background Motion Learner (BML) module that infers background motion representations from the latent features of the human pose sequence (as detailed in section 3.2). To further enhance the accuracy of background motion prediction, we incorporate epipolar masks derived from labeled camera trajectories as supervision (see section 3.3). Finally, the training objectives for AnimateAnywhere are described in section 3.4.

3.1 Preliminaries

Image-to-video CogVideoX Model. CogVideoX [34] is a video diffusion model with transformers (DiTs) that achieves high-quality video generation. Our AnimateAnyWhere is built upon the Image-to-Video framework of CogVideoX [34]. Given a condition image, CogVideoX [34] first pads it with zeros to N frames. Then the padded input is encoded by VAE and concatenated with noise. Subsequently, the combined latent is iteratively denoised over several steps to generate the final video. CogVideoX [34] employs unified 3D full attention modules within each DiT block. The 3D full attention module performs calculations simultaneously in spatial and temporal dimensions, capturing both intra-frame and cross-frame interactions. This enables CogVideoX [34] to comprehensively aggregate temporal information for video generation.

3D Full Attention. Firstly, the video latent $\mathbf{h} \in \mathbb{R}^{B \times F \times C \times H \times W}$ is reshaped as $\mathbf{h} \in \mathbb{R}^{B \times (H \times W \times F) \times C}$, where F , C , and (H, W) denote the temporal, channel, and spatial dimensions, respectively. And then the reshaped latent is input into the 3D Full Attention module. This 3D Full Attention module achieves a better understanding of video content by unifying the modeling of both time and space. The

attention map \mathbf{A} is computed as:

$$\mathbf{A} = \text{Softmax} \left(\frac{\mathbf{Q}(\mathbf{h})\mathbf{K}(\mathbf{h})^T}{\sqrt{d}} \right) \in \mathbb{R}^{B \times (H \times W \times F) \times (H \times W \times F)}, \quad (1)$$

where \mathbf{Q} and \mathbf{K} denote the query and key projections, respectively. The resulting attention map \mathbf{A} reflects the correspondences across video frames learned by the diffusion model.

3.2 AnimateAnywhere

As shown in fig. 2, AnimateAnywhere aims to simultaneously animate both the reference human and the reference background. The animation of the human is guided by the human pose sequence, while the background is guided by the implicit motion signals derived from the human pose sequence. Below, we describe the detailed process of human and background animation.

Human Animation. (1) Reference Human Input. To ensure that the human details are well preserved during animation, we introduce a ReferenceNet DiT, whose structure matches the first 18 blocks of the denoising DiT. Specifically, the reference human image is first encoded into latent space using a 3D VAE and subsequently passed through the ReferenceNet DiT to extract human features \mathbf{h}_{hum} . The human features are concatenated with the features from the main denoising DiT. These combined features are then processed through 3D full attention layers while preserving the original dimensions of the denoising DiT. **(2) Human Pose Sequence Guidance.** We adopt an architecture similar to ControlNet [18, 36] to guide human motion. Specifically, we replicate the first 18 blocks of the pre-trained denoising DiT to serve as the ControlNet DiT. We utilize the VAE encoder to transform the human pose sequence into latent features and then utilize the ControlNet DiT to extract multi-scale pose features $\mathbf{h}_{pose}^{1:N}$. Subsequently, these multi-scale features are added to the corresponding features of the denoising DiT via zero-initialized linear layers.

Background Animation. (1) Reference Background Input. Given a condition image, the CogVideoX [34] I2V model uses it as the first frame to generate a video. Following this setup, we treat the reference background as the condition image and the initial background of the generated video. The background image is initially padded to match the dimension of the video, then encoded into latent features via the VAE encoder, and finally concatenated with noise to serve as input for the DiT module. **(2) Background Motion Learner Module.** Unlike other methods that extract camera trajectories from reference videos as background motion signals, we propose to directly predict background motion from human pose sequences. An intuitive approach is to learn camera trajectories from human pose sequences and incorporate the learned camera trajectories during video generation. However, directly learning camera trajectories faces several challenges. First, a single human pose may correspond to multiple plausible camera trajectories due to the ambiguity of whether the human is moving or stationary. Moreover, the labeled camera trajectories often suffer from scale inconsistency, which also increases the optimization difficulty. In contrast, rather than explicitly decoupling camera trajectories, we directly utilize the background motion features embedded in human pose to drive background movement. In particular, we introduce a LoRA-based module named Background Motion Learner (BML) module into each DiT block, and this module follows the standard

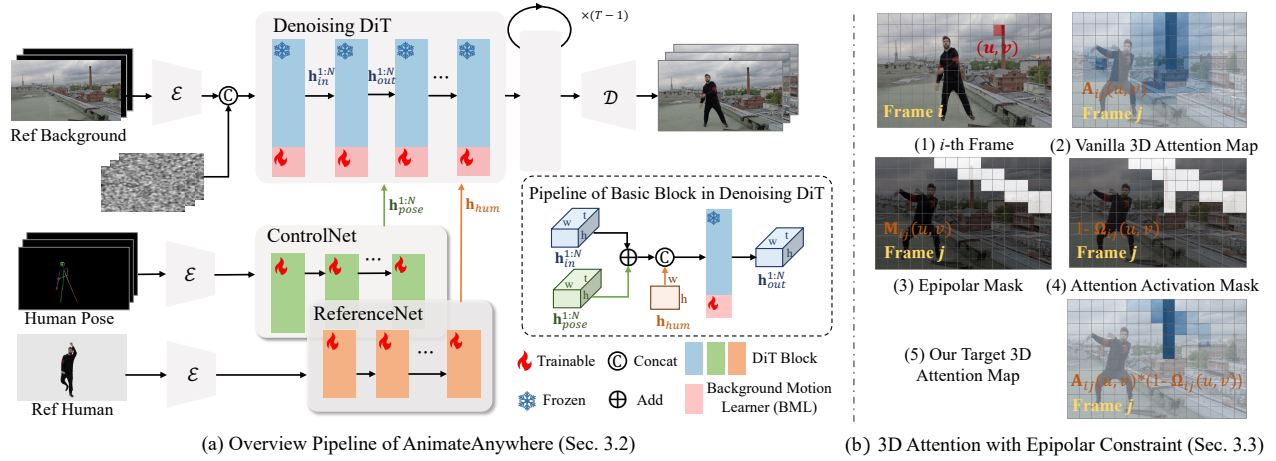


Figure 2: (a) Overview Pipeline of AnimateAnywhere. Given a reference background image, a reference human image, and a human pose sequence as inputs, AnimateAnywhere generates photorealistic videos with synchronized motion of both the human and the background. Built upon CogVideoX [34], we employ a ControlNet to inject human pose sequences and a ReferenceNet to incorporate the reference human. The background image is concatenated with noise to inject background appearance, while a Background Motion Learner (BML) predicts background motion from the pose sequence. (b) 3D Attention with Epipolar Constraint. (b)-(1) The i -th video frame. (b)-(2) Vanilla 3D attention map $A_{ij}(u, v)$ represents the model-learned attention weights from pixel (u, v) in the i -th frame to all positions in the j -th frame. (b)-(3) Epipolar mask $M_{ij}(u, v)$ defines the geometrically valid region in the j -th frame. (b)-(4) Attention activation mask $1 - \Omega_{ij}(u, v)$ highlights the retained attention regions without constraint. Adaptive suppression mask $\Omega_{ij}(u, v)$ selectively constrains low-confidence attention outside the epipolar region. (b)-(5) Target 3D attention map under our epipolar constraint. Our loss function is equivalent to computing the difference between $A_{ij}(u, v)$ and this target map.

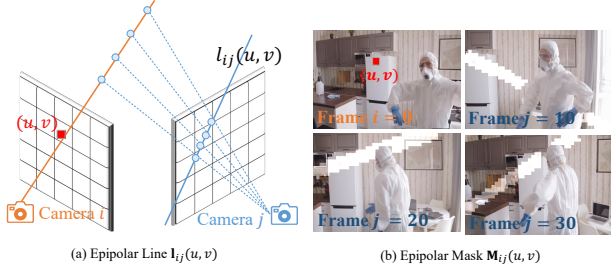


Figure 3: Epipolar line and epipolar mask. (a) The epipolar line $l_{ij}(u, v)$ is determined by the camera poses of the two frames. (b) The epipolar mask $M_{ij}(u, v)$ is defined at the resolution of the latent feature space.

paradigm of LoRA [11], expressed as $W_0x + \Delta Wx$. We add the human pose features h_{pose} and the denoising features h_{in} together to predict the background motion. The process is as follows:

$$h_{out}^{1:N} = T(h_{in}^{1:N} + h_{pose}^{1:N}) + B(h_{in}^{1:N} + h_{pose}^{1:N}), \quad (2)$$

where T and B denote DiT block and BML module. Specifically, h_{in} has strong priors on the co-movement between humans and backgrounds. h_{pose} , which is extracted from 3D attention in ControlNet, contains temporal information of human motion across frames.

3.3 Epipolar Constraint on 3D Attention Map

Although 3D full attention allows each background pixel to attend to any other pixel from all frames, this highly free search manner also makes optimization difficult and often causes geometric inconsistency in the background. To address this, we introduce epipolar

constraints into the 3D attention map. However, strictly restricting the correspondence search space to geometrically reasonable regions may undermine the cross-frame correlations learned by the original 3D full attention. So we propose an adaptive epipolar constraint that integrates an epipolar mask and the current 3D attention map. In the following, we first introduce the preliminaries of the epipolar constraint and the details of our proposed adaptive epipolar constraint on the 3D attention map.

Epipolar Line and Epipolar Mask. The camera poses consist of intrinsic parameters $K \in \mathbb{R}^{T \times 3 \times 3}$ and extrinsic parameters $[R; T]$, where $R \in \mathbb{R}^{T \times 3 \times 3}$ represents the rotational matrix and $T \in \mathbb{R}^{T \times 3 \times 1}$ denotes the translational matrix. The epipolar constraint establishes that a point (u, v) in the i -th frame must lie on its corresponding epipolar line $l_{ij}(u, v)$ in the j -th frame, as illustrated in fig. 3. The epipolar line can be determined by camera poses as:

$$l_{ij}(u, v) = F_{ij} \cdot (u, v, 1)^T, \quad (3)$$

where F_{ij} is the fundamental matrix between two frames. This matrix is computed as $F_{ij} = K_j^{-T} \cdot (T_{i \rightarrow j} \times R_{i \rightarrow j}) \cdot K_i^{-1}$. Here, $R_{i \rightarrow j} \in \mathbb{R}^{3 \times 3}$ and $T_{i \rightarrow j} \in \mathbb{R}^3$ are the relative rotation matrix and translation vector from i -th frame to j -th frame. Using the epipolar line, we convert each pixel (u', v') in the j -th frame into an epipolar mask $M_{ij}(u, v)$. The epipolar mask significantly reduces the number of matching points from hw (frame size) to l (where $l \ll hw$).

Adaptive Epipolar Constraint. We define the vanilla 3D attention map $A_{ij}(u, v)$ as the attention intensity, indicating how much the pixel (u, v) in the i -th frame attends to each position in the j -th

frame. As described above, the epipolar mask $\mathbf{M}_{ij}(u, v)$ strictly defines the valid region in the j -th frame that the pixel (u, v) in the i -th frame should correspond to under projective geometry. To ensure that background motion adheres to geometric constraints, for each background pixel (u, v) in i -th frame, we suppress the attention values of $\mathbf{A}_{ij}(u, v)$ that fall outside the corresponding epipolar region $\mathbf{M}_{ij}(u, v)$. However, completely suppressing attention outside the epipolar region $\mathbf{M}_{ij}(u, v)$ may disrupt the cross-frame correlations learned by 3D full attention. To mitigate this, we adaptively apply the epipolar constraint by incorporating a dynamic attention mask defined as $(\mathbf{A}_{ij}(u, v) < \delta)$, where $(\mathbf{A}_{ij}(u, v) < \delta)$ represents the region of low-confidence attention scores, *i.e.*, the regions the network itself tends to ignore. Thus, the suppressed regions are determined by the intersection: $\Omega_{ij}(u, v) = (1 - \mathbf{M}_{ij}(u, v)) \cap (\mathbf{A}_{ij}(u, v) < \delta)$. The final epipolar constraint is then defined by,

$$\mathcal{L}_{\text{epipolar}} = \sum_{i,j} \sum_{(u,v)} \Omega_{ij}(u, v) \cdot \mathbf{A}_{ij}(u, v), \quad (4)$$

where δ denotes a statistical threshold corresponding to the 30th percentile of attention values. Meanwhile, we emphasize that our loss function is equivalent to computing the difference between $\mathbf{A}_{ij}(u, v)$ and the target map, as illustrated in fig. 2 (b)-(5). During inference, our AnimateAnywhere no longer requires epipolar information or camera trajectories, and it directly leverages the attention learned through the epipolar loss.

3.4 Learning Objective

We employ the latent loss in CogVideoX [34] to train our pipeline,

$$\mathcal{L}_{\text{latent}} = \mathbb{E}_{z_0^{1:N}, \mathbf{t}, \mathbf{c}, \epsilon} [\|\epsilon - \epsilon_\theta(z_t^{1:N}, \mathbf{t}, \mathbf{c})\|_2^2], \quad (5)$$

where ϵ_θ denotes our diffusion model, $z_0^{1:N}$ represents the latent embeddings of an N -frame image sequence, and $z_t^{1:N}$ corresponds to the noisy latent at diffusion timestep t . The variable \mathbf{c} denotes the conditioning inputs provided to our model, specifically including \mathbf{I}_{hum} , \mathbf{I}_{bg} , and $\mathbf{P}^{1:N}$, while ϵ denotes the unscaled noise.

Meanwhile, we employ a one-step sampling strategy to transform the predicted latent $z_t^{1:N}$ at timestep \mathbf{t} to $z_0^{1:N}$ and we decode $z_0^{1:N}$ into the RGB video $\mathbf{V}^{1:N}$ through the VAE decoder. We employ the VGG perceptual loss between the generated frames $\hat{\mathbf{V}}^{1:N}$ and the target frames $\mathbf{V}^{1:N}$ during the last 30% timesteps as follow:

$$\mathcal{L}_{\text{vgg}} = (1 + \mathbf{m}) * \text{VGG}(\hat{\mathbf{V}}^{1:N}, \mathbf{V}^{1:N}), \quad (6)$$

where \mathbf{m} is the mask sequence of the human hand region.

The overall learning objective for training is defined by,

$$\mathcal{L} = \mathcal{L}_{\text{latent}} + \lambda_{\text{vgg}} \mathcal{L}_{\text{vgg}} + \lambda_{\text{epipolar}} \mathcal{L}_{\text{epipolar}} \quad (7)$$

where λ_{vgg} and $\lambda_{\text{epipolar}}$ are the weights to balance the loss terms.

4 Experiments

4.1 Experimental Details

Dataset. We collect 5K videos from the Humanvid [28] dataset and 3K videos from the Internet for training, where the Humanvid [28] dataset has the annotation of camera pose sequence. Our training dataset consists of videos captured under diverse camera conditions, including both static and moving cameras.

We evaluate our model on the Humanvid [28] test dataset and a wild dataset, Bilibili200 (BL200), collected from the internet. The Humanvid test dataset includes 100 videos with noticeable background motion but limited human motion. The BL200 dataset contains 200 videos with significant motion in both the human and background.

For fair comparison, we evaluate all methods by generating 48-frame sequences with a stride of 4. Notably, while other methods utilize a single reference image that contains both the human and background during testing, our method inputs the reference human and reference background separately.

Evaluation Metrics. Following the metrics utilized in [12, 24, 25, 32, 40, 42], we use PSNR [14], SSIM [27], and LIPIS [37] metrics to evaluate the quality of single-frame images. Additionally, we introduce FID [7] and FVD [23] metrics to evaluate the difference between the distributions of generated videos and real-world videos.

Implementation Details. We adopt the pretrained CogVideoX1.5-5B-I2V [34] as our base model and keep it frozen throughout the training process. Both ControlNet and ReferenceNet are initialized with the parameters of CogVideoX [34]. Our training consists of three stages. In the first stage, we incorporate ControlNet into the base model and train only ControlNet while keeping all other parameters fixed. In the second stage, we introduce ReferenceNet and train it exclusively. In the final stage, we jointly optimize ControlNet, ReferenceNet, and the BML module.

In terms of data preparation, we first employ Grounded-SAM [19] to extract mask sequences in the human body and hand regions for each video. Subsequently, we obtain the human sequence and the background sequence using the extracted mask sequence. We randomly select a frame in the human sequence as the reference human and take the first frame from the background sequence as the reference background. Specifically, we complete the reference background using the inpainting method [41]. All experiments are trained on a mixture of horizontal (1360×768) and vertical (768×1360) videos and conducted on two A100 GPUs. Training is performed over 20,000 steps with a batch size of 8. We employ the AdamW optimizer [16] with a constant learning rate of 1×10^{-5} . We set the trade-off weights λ_{vgg} and $\lambda_{\text{epipolar}}$ to 0.2 and 0.005, respectively. During inference, classifier-free guidance (CFG) is applied with a scale of 2.5 for both reference images and pose sequences.

4.2 Comparison with Existing Methods

We compare our method with existing state-of-the-art human animation methods in both quantitative and qualitative aspects, including MagicAnimate [32], AnimateAnyone [12], Champ [42], MusePose [22], and HumanVid [28]. Since AnimateAnyone [12] is not officially open-sourced, we adopt its publicly available reimplementation from Moore-AnimateAnyone¹ for evaluation. Note that these methods, except HumanVid [28], are originally trained on datasets with static backgrounds. For fair comparison, we retrain AnimateAnyone [12] and MusePose [22] on our training dataset. In addition, Humanvid [28] is capable of generating dynamic backgrounds, similar to ours. As its official implementation is not released, we reimplement Humanvid [28] according to the details mentioned in its paper.

¹<https://github.com/MooreThreads/Moore-AnimateAnyone>

Table 1: Quantitative comparison for human animate on Humanvid [28] test dataset and BL200 dataset. The best results are highlighted with bold. Results marked by † and ‡ are retrained or reproduced with the Humanvid [28] train dataset, respectively. Since the BL200 test dataset lacks labeled camera poses, the results of Humanvid‡ [28] are not available.

Methods	HumanVid					BL200				
	PSNR↑	SSIM↑	LIPIS↓	FID↓	FVD↓	PSNR↑	SSIM↑	LIPIS↓	FID↓	FVD↓
MagicAnimate [32]	16.01	0.5463	0.4455	78.01	1943.07	16.82	0.5914	0.4133	40.02	1884.48
AnimateAnyone [12]	16.47	0.5311	0.3913	50.18	1431.43	17.58	0.5756	0.3635	24.46	1507.05
Champ [42]	15.08	0.5075	0.4481	63.92	1837.07	16.88	0.5649	0.3919	30.69	1701.45
MusePose [22]	16.93	0.5578	0.3676	52.00	1784.85	18.67	0.6126	0.3220	22.86	1580.47
AnimateAnyone† [12]	16.81	0.5486	0.3672	47.69	1235.65	18.23	0.5930	0.3379	23.27	1371.22
MusePose† [22]	17.33	0.5629	0.3563	44.73	1362.14	18.60	0.6116	0.3245	22.09	1444.79
Humanvid‡ [28]	16.42	0.5242	0.3676	47.41	1114.55	-	-	-	-	-
Ours	18.07	0.5831	0.3119	44.51	978.09	18.99	0.6182	0.3206	21.31	1154.27

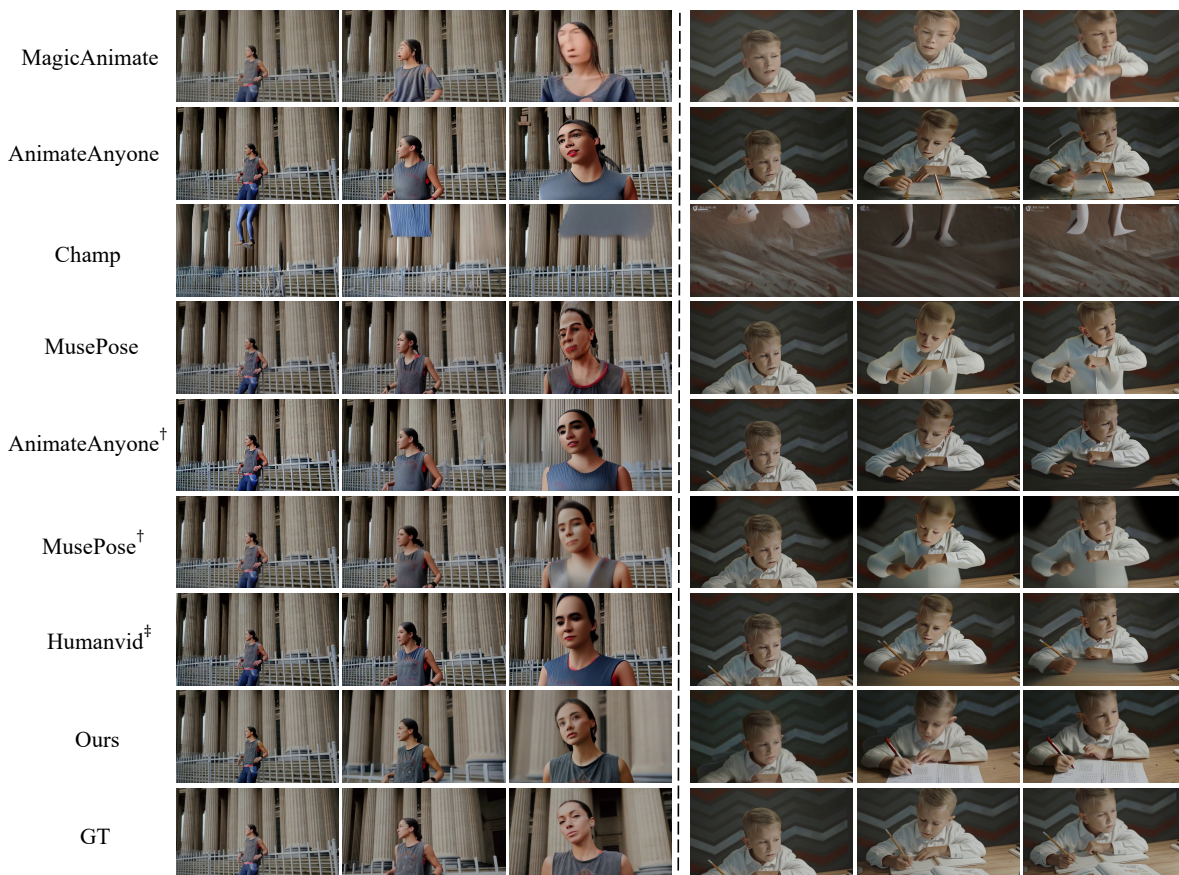


Figure 4: Qualitative comparison on Humanvid [28] test dataset. Our proposed method generates more realistic videos while ensuring harmonious motion between the foreground and background. Champ [42] predicts SMPL parameters, including camera parameters, but when the camera moves significantly, the estimated camera parameters become unreliable.

Quantitative Comparison. We conduct comprehensive experiments to assess the effectiveness of the proposed method, and the quantitative results are shown in table 1. From all metrics on the Humanvid [28] test dataset and the BL200 test dataset, we can see that previous methods struggle to generate videos with dynamic backgrounds, resulting in the difference between the dynamic ground-truth videos. Even the retrained versions of these

baselines occasionally produce static backgrounds, as they are not properly designed for background motion synchronized with human poses. In contrast, our method leverages CogVideoX [34], the BML, and the epipolar loss to achieve substantial improvements, outperforming all baselines in reconstruction metrics. Furthermore, it also achieves state-of-the-art video fidelity, improving FID by 6% and FVD by 12% over the strongest baseline.

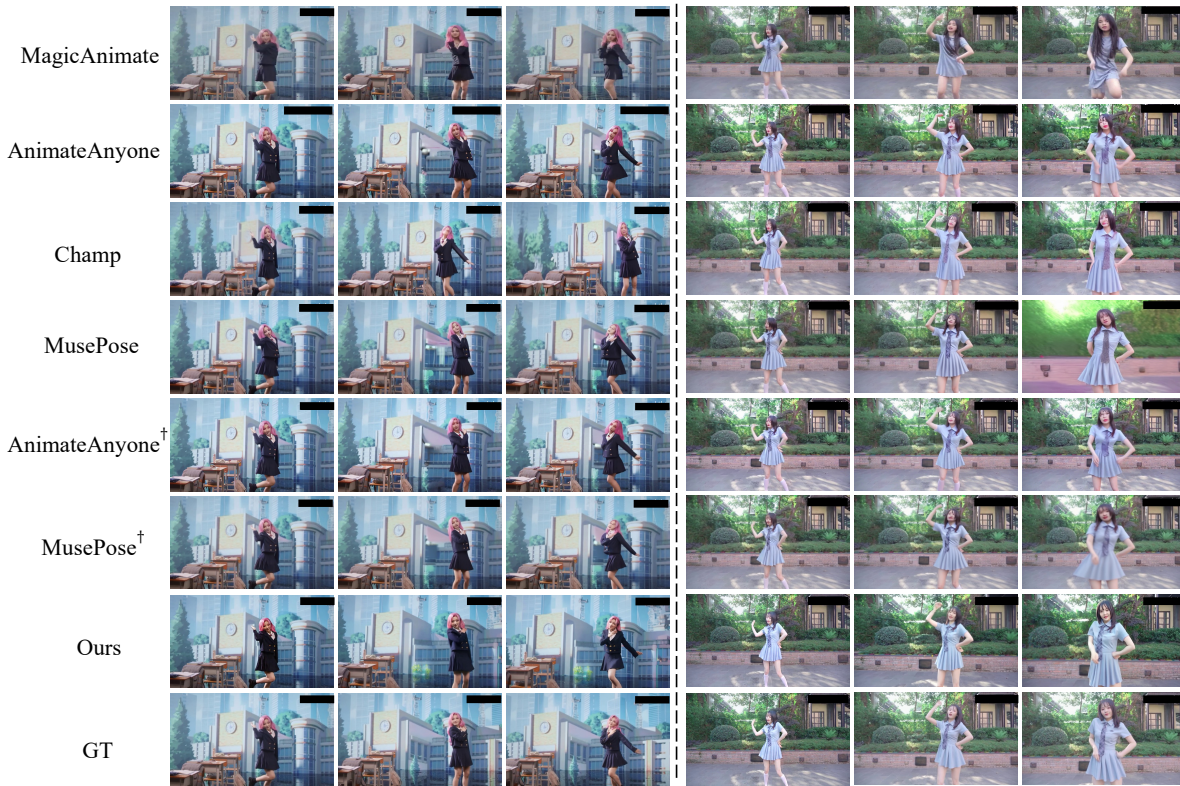


Figure 5: Qualitative comparisons on the BL200 test dataset. Our method not only generates realistic background motion but also maintains the temporal consistency of both the human and background.

Table 2: Ablation study on the epipolar loss $\mathcal{L}_{epipolar}$.

	PSNR \uparrow	SSIM \uparrow	LIPIS \downarrow	FID \downarrow	FVD \downarrow
Ours w/o $\mathcal{L}_{epipolar}$	18.06	0.5807	0.3246	45.22	981.37
Ours with $\mathcal{L}_{epipolar} (1 - M)$	17.32	0.5697	0.3280	50.81	1070.79
Ours with $\mathcal{L}_{epipolar} ((1 - M) \cap (A < \delta))$	18.07	0.5831	0.3119	44.51	978.09

Qualitative Comparison. The qualitative comparison with competing methods is shown in fig. 4. MagicAnimate [32], AnimateAnyone [12], Champ [42], and MusePose [22] generate videos with static backgrounds that are usually unrealistic and exhibit various artifacts. Even after retraining, these methods show limited improvements and still fail in some circumstances. For instance, the left example exhibits the static background, while the right example produces an inharmonious scene in which only the wall moves and the table remains motionless. Humanvid is more likely to generate dynamic backgrounds, yet the background motion is frequently misaligned with the human. In the left example, the background moves noticeably slower than the person. In contrast, our method synthesizes photorealistic videos while maintaining coherent motion between the human and the background. fig. 5 illustrates more generated videos on BL200 dataset. These results also highlight our method’s capability to generate realistic background motion while maintaining high-quality, temporally consistent animation of both the human and the background. Moreover, our method achieves better identity-preserving than other methods.

Animation Cross Human and Background. Existing methods typically rely on a single reference image that includes both the

human and the background, which limits the ability to customize videos for individual characters and backgrounds. In contrast, our method allows for separate input of the reference human and the reference background, enhancing the flexibility of the generation process. To validate the effectiveness of our approach, we present additional results of different characters and backgrounds in fig. 6, further confirming the unique advantages of our method.

5 Ablation Study

Effects of Epipolar Loss. As shown in fig. 7, the generated video exhibits noticeable artifacts in the background without incorporating epipolar loss, because the learned background motion does not adhere to geometric constraints. Additionally, suppressing all attention values outside the epipolar mask does not alleviate this issue but performs even worse. As evidenced in the second row of fig. 7, noticeable artifacts and unexpected objects appear in the background. In contrast, our approach achieves desired results by applying $\mathcal{L}_{epipolar}$ to the region of $(1 - M) \cap (A < \delta)$. As shown in table 2, our method with $\mathcal{L}_{epipolar} (1 - M) \cap (A < \delta)$ outperforms both the one without epipolar loss and the one using the mask $(1 - M)$, demonstrating its effectiveness.

Effects of VGG Loss. We investigate the impact of the VGG perceptual loss \mathcal{L}_{vgg} on video generation. While the 3D VAE used in CogVideoX [34] achieves efficient spatiotemporal compression (8× spatially, 4× temporally), we observe that optimizing solely with an L2 loss in latent space leads to degraded high-frequency details. As

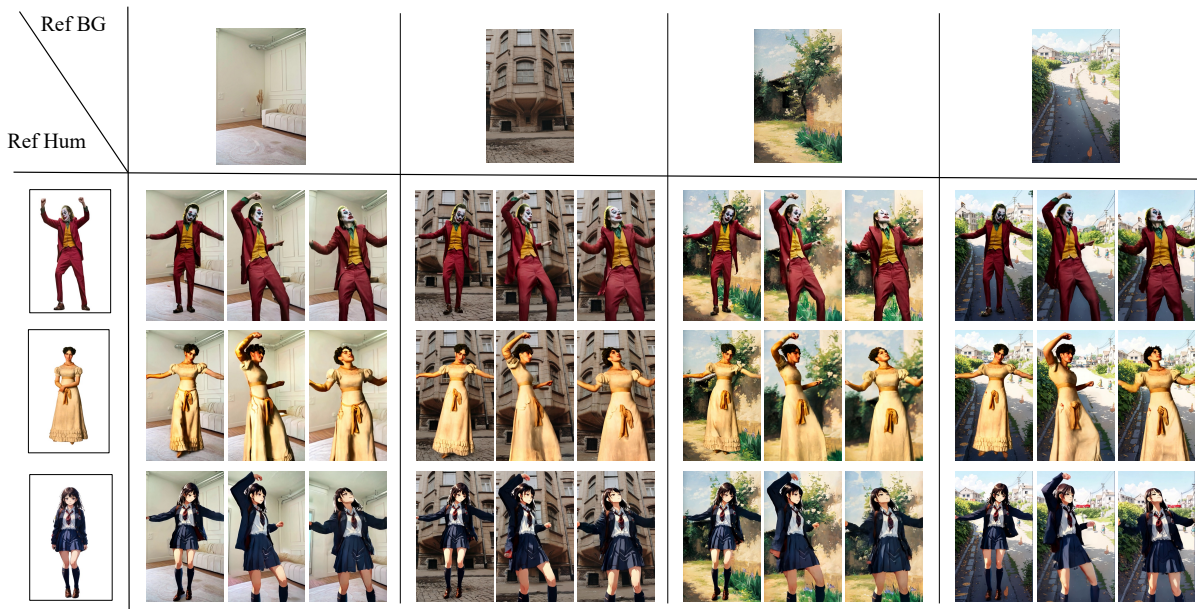


Figure 6: The results are obtained from our method by cross-using the reference human image and background image.



Figure 7: Qualitative comparison of epipolar loss. Without the epipolar loss or with $(1 - M)$, the background contains obvious artifacts highlighted by the red box. In contrast, our proposed epipolar loss yields the most consistent background.

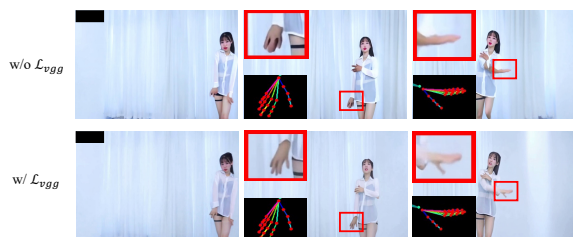


Figure 8: The generated results with and without the VGG perceptual loss. The result with VGG perceptual loss better preserves the fine details highlighted by the red box.

shown in fig. 8, the hand regions exhibit blurred contours without \mathcal{L}_{vgg} . After incorporating \mathcal{L}_{vgg} in pixel space, the details of the hand regions are well-preserved.

Effects of Foundational Models. To validate the superiority of our base model CogVideoX [34], we select several state-of-the-art video generation base models (AnimateDiff [4], SVD [2]) for comparison. Specifically, we build two new pipelines based on AnimateDiff [28] and SVD [2], and train them using our training dataset. Although these pipelines can generate videos with dynamic

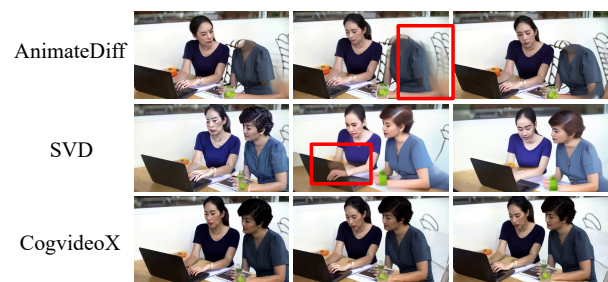


Figure 9: Visual comparison for different foundational frameworks based on the Humanvid [28] dataset.

backgrounds, they struggle with the generation of novel regions. For instance, as shown in fig. 9, the pipeline based on AnimateDiff [4] generates blurred novel regions, while the pipeline based on SVD [2] yields unnatural human parts. In contrast, our method, based on CogvideoX [34], successfully addresses these challenges.

6 Conclusion

In this paper, we introduce AnimateAnywhere, a human animation framework that generates videos with synchronized human and background motion without requiring specific background motion controls. The core of our framework is learning background motion representations directly from human pose sequences. Our method also provides additional geometric constraints on background motion learning by leveraging the labeled camera poses during training. Extensive experiments across multiple benchmarks validate the effectiveness of our AnimateAnywhere, demonstrating state-of-the-art performance in creating dynamic, realistic backgrounds that harmonize with human motion. This innovation not only improves the realism of the generated videos but also opens new possibilities in applications such as entertainment, virtual reality, and artistic content creation, where dynamic and immersive human-centered animations are increasingly valuable.

References

- [1] Omer Bar-Tal, Hila Chefer, Omer Tov, Charles Herrmann, Roni Paiss, Shiran Zada, Ariel Ephrat, Junhwa Hur, Guanghui Liu, Amit Raj, et al. 2024. Lumiere: A space-time diffusion model for video generation. *arXiv preprint arXiv:2401.12945* (2024).
- [2] Andreas Blattmann, Tim Dockhorn, Sumith Kulal, Daniel Mendeleevitch, Maciej Kilian, Dominik Lorenz, Yam Levi, Zion English, Vikram Voleti, Adam Letts, et al. 2023. Stable video diffusion: Scaling latent video diffusion models to large datasets. *arXiv preprint arXiv:2311.15127* (2023).
- [3] Yuwei Guo, Ceyuan Yang, Anyi Rao, Maneesh Agrawala, Dahua Lin, and Bo Dai. 2025. Sparsectrl: Adding sparse controls to text-to-video diffusion models. In *European Conference on Computer Vision*. Springer, 330–348.
- [4] Yuwei Guo, Ceyuan Yang, Anyi Rao, Zhengyang Liang, Yaohui Wang, Yu Qiao, Maneesh Agrawala, Dahua Lin, and Bo Dai. 2023. Animatediff: Animate your personalized text-to-image diffusion models without specific tuning. *arXiv preprint arXiv:2307.04725* (2023).
- [5] Agrim Gupta, Lijun Yu, Kihyuk Sohn, Xiuyu Gu, Meera Hahn, Fei-Fei Li, Irfan Essa, Lu Jiang, and José Lezama. 2025. Photorealistic video generation with diffusion models. In *European Conference on Computer Vision*. Springer, 393–411.
- [6] Hao He, Yinghao Xu, Yuwei Guo, Gordon Wetzstein, Bo Dai, Hongsheng Li, and Ceyuan Yang. 2024. Cameractrl: Enabling camera control for text-to-video generation. *arXiv preprint arXiv:2404.02101* (2024).
- [7] Martin Heusel, Hubert Ramsauer, Thomas Unterthiner, Bernhard Nessler, and Sepp Hochreiter. 2017. Gans trained by a two time-scale update rule converge to a local nash equilibrium. *Advances in neural information processing systems* 30 (2017).
- [8] Jonathan Ho, Tim Salimans, Alexey Gritsenko, William Chan, Mohammad Norouzi, and David J Fleet. 2022. Video diffusion models. *Advances in Neural Information Processing Systems* 35 (2022), 8633–8646.
- [9] Chen Hou, Guoqiang Wei, Yan Zeng, and Zhibo Chen. 2024. Training-free Camera Control for Video Generation. *arXiv preprint arXiv:2406.10126* (2024).
- [10] Edward J Hu, Yelong Shen, Phillip Wallis, Zeyuan Allen-Zhu, Yuanzhi Li, Shean Wang, Lu Wang, and Weizhu Chen. 2021. Lora: Low-rank adaptation of large language models. *arXiv preprint arXiv:2106.09685* (2021).
- [11] Edward J Hu, Yelong Shen, Phillip Wallis, Zeyuan Allen-Zhu, Yuanzhi Li, Shean Wang, Lu Wang, Weizhu Chen, et al. 2022. Lora: Low-rank adaptation of large language models. *ICLR* 1, 2 (2022), 3.
- [12] Li Hu. 2024. Animate anyone: Consistent and controllable image-to-video synthesis for character animation. In *Proceedings of the IEEE/CVF Conference on Computer Vision and Pattern Recognition*. 8153–8163.
- [13] Li Hu, Guangyuan Wang, Zhen Shen, Xin Gao, Dechao Meng, Lian Zhuo, Peng Zhang, Bang Zhang, and Liefeng Bo. 2025. Animate Anyone 2: High-Fidelity Character Image Animation with Environment Affordance. *arXiv preprint arXiv:2502.06145* (2025).
- [14] Quan Huynh-Thu and Mohammed Ghanbari. 2008. Scope of validity of PSNR in image/video quality assessment. *Electronics letters* 44, 13 (2008), 800–801.
- [15] Jinlin Liu, Kai Yu, Mengyang Feng, Xiefang Guo, and Miaomiao Cui. 2024. Disentangling Foreground and Background Motion for Enhanced Realism in Human Video Generation. *arXiv preprint arXiv:2405.16393* (2024).
- [16] Ilya Loshchilov and Frank Hutter. 2017. Decoupled weight decay regularization. *arXiv preprint arXiv:1711.05101* (2017).
- [17] Yifang Men, Yuan Yao, Miaomiao Cui, and Liefeng Bo. 2024. Mimo: Controllable character video synthesis with spatial decomposed modeling. *arXiv preprint arXiv:2409.16160* (2024).
- [18] Chong Mou, Xintao Wang, Liangbin Xie, Yanze Wu, Jian Zhang, Zhongang Qi, and Ying Shan. 2024. T2i-adapter: Learning adapters to dig out more controllable ability for text-to-image diffusion models. In *Proceedings of the AAAI Conference on Artificial Intelligence*, Vol. 38. 4296–4304.
- [19] Tianhe Ren, Shilong Liu, Ailing Zeng, Jing Lin, Kunchang Li, He Cao, Jiayu Chen, Xinyu Huang, Yukang Chen, Feng Yan, Zhaoyang Zeng, Hao Zhang, Feng Li, Jie Yang, Hongyang Li, Qing Jiang, and Lei Zhang. 2024. Grounded SAM: Assembling Open-World Models for Diverse Visual Tasks. *arXiv:2401.14159* [cs.CV]
- [20] Shuai Tan, Biao Gong, Xiang Wang, Shiwei Zhang, Dandan Zheng, Ruobing Zheng, Kecheng Zheng, Jingdong Chen, and Ming Yang. 2024. Animate-X: Universal Character Image Animation with Enhanced Motion Representation. *arXiv preprint arXiv:2410.10306* (2024).
- [21] Zachary Teed and Jia Deng. 2021. Droid-slam: Deep visual slam for monocular, stereo, and rgb-d cameras. *Advances in neural information processing systems* 34 (2021), 16558–16569.
- [22] Zhengyan Tong, Chao Li, Zhaokang Chen, Bin Wu, and Wenjiang Zhou. 2024. MusePose: a Pose-Driven Image-to-Video Framework for Virtual Human Generation. *arxiv* (2024).
- [23] Thomas Unterthiner, Sjoerd van Steenkiste, Karol Kurach, Raphaël Marinier, Marcin Michalski, and Sylvain Gelly. 2019. FVD: A new metric for video generation. (2019).
- [24] Benzhi Wang, Jingkai Zhou, Jingqi Bai, Yang Yang, Weihua Chen, Fan Wang, and Zhen Lei. 2024. RealisHuman: A Two-Stage Approach for Refining Malformed Human Parts in Generated Images. *arXiv preprint arXiv:2409.03644* (2024).
- [25] Xiang Wang, Shiwei Zhang, Changxin Gao, Jiayu Wang, Xiaoqiang Zhou, Yingya Zhang, Luxin Yan, and Nong Sang. 2024. UniAnimate: Taming Unified Video Diffusion Models for Consistent Human Image Animation. *arXiv preprint arXiv:2406.01188* (2024).
- [26] Yufu Wang, Ziyun Wang, Lingjie Liu, and Kostas Daniilidis. 2024. TRAM: Global Trajectory and Motion of 3D Humans from in-the-wild Videos. *arXiv preprint arXiv:2403.17346* (2024).
- [27] Zhou Wang, Alan C Bovik, Hamid R Sheikh, and Eero P Simoncelli. 2004. Image quality assessment: from error visibility to structural similarity. *IEEE transactions on image processing* 13, 4 (2004), 600–612.
- [28] Zhenzhi Wang, Yixuan Li, Yanhong Zeng, Youqing Fang, Yuwei Guo, Wenran Liu, Jing Tan, Kai Chen, Tianfan Xue, Bo Dai, et al. 2024. HumanVid: Demystifying Training Data for Camera-controllable Human Image Animation. *arXiv preprint arXiv:2407.17438* (2024).
- [29] Zhouxia Wang, Ziyang Yuan, Xintao Wang, Yaowei Li, Tianshui Chen, Menghan Xia, Ping Luo, and Ying Shan. 2024. Motionctrl: A unified and flexible motion controller for video generation. In *ACM SIGGRAPH 2024 Conference Papers*. 1–11.
- [30] Yujie Wei, Shiwei Zhang, Zhiwu Qing, Hangjie Yuan, Zhiheng Liu, Yu Liu, Yingya Zhang, Jingren Zhou, and Hongming Shan. 2024. Dreamvideo: Composing your dream videos with customized subject and motion. In *Proceedings of the IEEE/CVF Conference on Computer Vision and Pattern Recognition*. 6537–6549.
- [31] Dejia Xu, Wei Nie, Chao Liu, Sifei Liu, Jan Kautz, Zhangyang Wang, and Arash Vahdat. 2024. CamCo: Camera-Controllable 3D-Consistent Image-to-Video Generation. *arXiv preprint arXiv:2406.02509* (2024).
- [32] Zhongcong Xu, Jianfeng Zhang, Jun Hao Liew, Hanshu Yan, Jia-Wei Liu, Chenxu Zhang, Jiashi Feng, and Mike Zheng Shou. 2024. Magicanimate: Temporally consistent human image animation using diffusion model. In *Proceedings of the IEEE/CVF Conference on Computer Vision and Pattern Recognition*. 1481–1490.
- [33] Shiyuan Yang, Liang Hou, Haibin Huang, Chongyang Ma, Pengfei Wan, Di Zhang, Xiaodong Chen, and Jing Liao. 2024. Direct-a-video: Customized video generation with user-directed camera movement and object motion. In *ACM SIGGRAPH 2024 Conference Papers*. 1–12.
- [34] Zhuoyi Yang, Jiayan Teng, Wendi Zheng, Ming Ding, Shiyu Huang, Jiazheng Xu, Yuanming Yang, Wenyi Hong, Xiaohan Zhang, Guanyu Feng, et al. 2024. Cogvideox: Text-to-video diffusion models with an expert transformer. *arXiv preprint arXiv:2408.06072* (2024).
- [35] Mingshuai Yao, Mengting Chen, Qinye Zhou, Yabo Zhang, Ming Liu, Xiaoming Li, Shaohui Liu, Chen Ju, Shuai Xiao, Qingwen Liu, et al. 2025. Beyond Static Scenes: Camera-controllable Background Generation for Human Motion. *arXiv preprint arXiv:2504.02004* (2025).
- [36] Lvmin Zhang, Anyi Rao, and Maneesh Agrawala. 2023. Adding conditional control to text-to-image diffusion models. In *Proceedings of the IEEE/CVF International Conference on Computer Vision*. 3836–3847.
- [37] Richard Zhang, Phillip Isola, Alexei A Efros, Eli Shechtman, and Oliver Wang. 2018. The unreasonable effectiveness of deep features as a perceptual metric. In *Proceedings of the IEEE conference on computer vision and pattern recognition*. 586–595.
- [38] Yabo Zhang, Yuxiang Wei, Dongsheng Jiang, Xiaopeng Zhang, Wangmeng Zuo, and Qi Tian. 2023. Controlvideo: Training-free controllable text-to-video generation. *arXiv preprint arXiv:2305.13077* (2023).
- [39] Guangcong Zheng, Teng Li, Rui Jiang, Yehao Lu, Tao Wu, and Xi Li. 2024. Cami2v: Camera-controlled image-to-video diffusion model. *arXiv preprint arXiv:2410.15957* (2024).
- [40] Jingkai Zhou, Benzhi Wang, Weihua Chen, Jingqi Bai, Dongyang Li, Aixi Zhang, Hao Xu, Mingyang Yang, and Fan Wang. 2024. RealisDance: Equip controllable character animation with realistic hands. *arXiv preprint arXiv:2409.06202* (2024).
- [41] Shangchen Zhou, Chongyi Li, Kelvin C.K Chan, and Chen Change Loy. 2023. ProPainter: Improving Propagation and Transformer for Video Inpainting. In *Proceedings of IEEE International Conference on Computer Vision (ICCV)*.
- [42] Shenhao Zhu, Junming Leo Chen, Zuozhuo Dai, Yinghui Xu, Xun Cao, Yao Yao, Hao Zhu, and Siyu Zhu. 2024. Champ: Controllable and consistent human image animation with 3d parametric guidance. *arXiv preprint arXiv:2403.14781* (2024).